Off-axis electron holography and image spectroscopy of ferromagnetic FeNi nanoparticles

R K K Chong[1], R E Dunin-Borkowski[1], T Kasama[1,2], M J Hÿtch[3] and M R McCartney[4]

[1] Department of Materials Science and Metallurgy, University of Cambridge, Cambridge CB2 3QZ, UK

[2] RIKEN (The Institute of Physical and Chemical Research), 2-1 Hirosawa, Wako, Saitama 351-0198, Japan

[3] Centre d'Etudes de Chimie Métallurgique - CNRS, 15 rue G. Urbain, 94407 Vitry-sur-Seine, France

[4] Center For Solid State Science, Arizona State University, Tempe, AZ 85287-1704, USA

Abstract. The magnetic remanent states and chemical compositions of chains of crystalline Fe_xNi_{1-x} nanoparticles, which have an average size of 50 nm, have been characterised using off-axis electron holography and image spectroscopy. The critical sizes at which the particles can support magnetic vortices are correlated with their compositions. A significant increase in magnetic vortex core diameter is observed when vortices in the nanoparticles are aligned parallel to the chain axes.

1. Introduction

The magnetic properties of closely-spaced nanoparticles are of considerable interest, both fundamentally and for the design of ultra-high-density magnetic devices. However, the factors that influence the critical sizes at which such particles begin to support complicated domain structures, rather than single magnetic domains, are poorly understood. Such effects are difficult to predict theoretically because of the large number of variable parameters that need to be included in simulations of the magnetic microstructure of a distribution of nanoparticles, which is sensitive not only to magnetostatic interactions between each particle and its neighbours and to the magnetic history of the specimen but also to the morphologies and the compositions of the individual particles. Here, we use image spectroscopy[1] and off-axis electron holography[2] to characterise linear chains of crystalline nanoparticles that have an average diameter of 50 nm, nominal compositions of $Fe_{55}Ni_{45}$, $Fe_{30}Ni_{70}$ or $Fe_{10}Ni_{90}$, and 4-nm-thick oxide layers surrounding their metal cores. We begin by assessing the accuracy and the precision to which the nanoparticle compositions can be measured using image spectroscopy. We then correlate these measurements with the magnetic microstructures of individual nanoparticle chains, which are measured using electron holography.

2. Image Spectroscopy

Image spectroscopy involves the analysis of an extended series of energy-loss images, and allows the formation of chemical maps of materials with better signal to noise than using three-window elemental mapping. Approaches that are normally applied to electron energy-loss spectra can then be used to improve the fitting parameters for the energy loss background at each image pixel, as well as allowing the deconvolution of plural scattering effects and the use of large energy-selecting windows without introducing additional chromatic blurring. Figure 1a shows part of a series of energy-loss images of two $Fe_{55}Ni_{45}$ nanoparticle chains acquired at 300 kV on a Philips CM300 field emission gun transmission electron microscope (FEGTEM) equipped with a Gatan imaging filter. Energy losses of 0-1200 eV were used, with an energy-selecting slit width of 20 eV and an interval of 20 eV between images. The pixel size is 2.4 nm. Figure 1b shows the corresponding energy-loss spectrum averaged over all image pixels, while Fig. 1c shows O and Fe chemical maps derived from the O K and Fe $L_{2,3}$ edges using optimal pre and post edge windows. The 4 nm oxide shell is visible around each particle in the O map, while diffraction contrast is visible in both signals. Figure 1e shows the Fe/Ni ratios in several nanoparticles in each sample, calculated using a 60 eV pre-edge window, several post-edge window sizes and Hartree-Slater cross-sections[3].

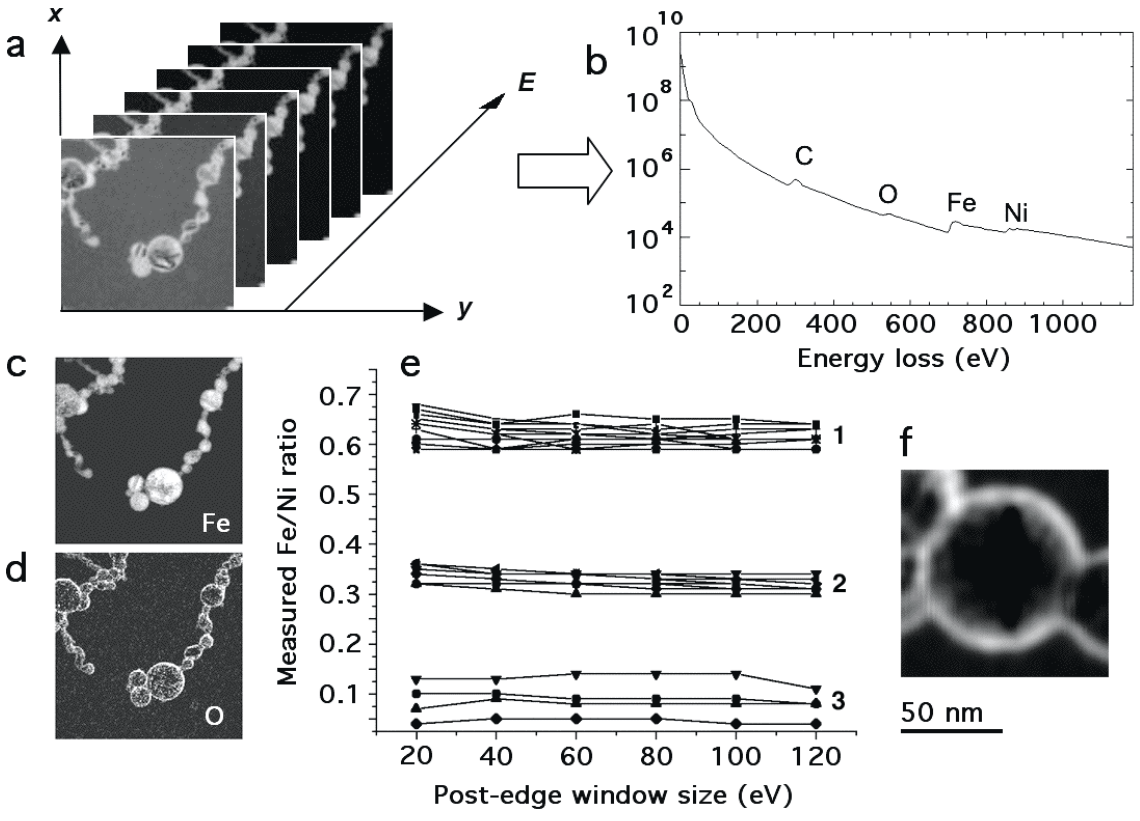

Figure 1 a) Image spectroscopy data from $Fe_{55}Ni_{45}$ nanoparticles. b) Energy-loss spectrum derived from a). c) - d) Elemental maps derived from the Fe $L_{2,3}$ and O K edges. e) Image spectroscopy measurements of Fe/Ni ratios in several nanoparticles in samples of nominal composition: 1. $Fe_{55}Ni_{45}$, 2. $Fe_{30}Ni_{70}$ and 3. $Fe_{10}Ni_{90}$, plotted vs. post-edge window size starting at the Fe and Ni $L_{2,3}$ edge thresholds. f) Oxygen map, showing faceting around a 75 nm nanoparticle, after sub-pixel alignment of the images.

The consistency between the measurements from different nanoparticles in the same sample is better than expected, presumably because some of the possible sources of random and systematic error in the measurements, such as those associated with diffraction contrast and errors in the calculated scattering factors, cancel out when a ratio between the Fe and Ni signals is calculated. The measured Fe/Ni ratios are on average 0.63±0.03, 0.33±0.03 and 0.09±0.03 for the samples that have nominal ratios of 0.55, 0.30 and 0.10, respectively. A slight decrease in these values is sometimes observed with increasing post-edge window size, perhaps because of the inadequate treatment of Fe and Ni white lines in the calculated cross-sections. Although our results confirm the broad trend in the particle compositions, further systematic errors, which are presently being investigated, almost certainly remain. The errors may be associated with the oxide shell around each particle having a different composition from the core, with the presence of the Fe L_1 edge at the position of the Ni $L_{2,3}$ edge in the energy-loss spectrum, and with plural scattering in the largest particles. A final difficulty results from the need to perform sub-pixel alignment of the original images. Only after this procedure is performed is faceting of the particles revealed in the O maps (Fig.1e).

3. Off-Axis Electron Holography

Off-axis electron holograms of the nanoparticle chains were acquired either at 300 kV using a Philips CM300ST FEGTEM or at 200 kV using a Philips CM200ST FEGTEM. Each microscope was equipped with a 'Lorentz' lens, which allows the magnetic microstructure in the samples to be recorded in field-free conditions at high spatial resolution. The technique involves applying a voltage to an electron biprism in order to overlap a coherent electron wave that has passed through the sample with a part of the same electron wave that has passed only through vacuum. Analysis of the resulting interference pattern allows the phase shift of the electron wave to be recovered quantitatively and non-invasively at a spatial resolution close to the nm scale [2].

Figures 2a and b show the magnetic remanent states of two chains of $Fe_{55}Ni_{45}$ particles, which have been measured using electron holography. The density of the contours is proportional to the in-plane induction in the sample integrated in the electron beam direction, and the spatial resolution of the magnetic information is estimated to be approximately 10 nm. The unwanted mean inner potential (MIP) contribution to the phase shift (which provides a value of 21.5±0.3 V for the MIP in each sample) has been subtracted from the images [2]. The remanent state of a 75 nm $Fe_{55}Ni_{45}$ particle sandwiched between two smaller particles is shown in Fig. 2a. Closely-spaced contours run through all three particles in a channel of width 22±4 nm. Comparisons with simulations suggest that the largest particle contains a vortex whose axis lies parallel to the chain axis, as shown schematically in Fig. 2c. The lack of contours on either side of the flux channel that forms the vortex core results from the induction in these regions being substantially out-of-plane. In Fig. 2b, a vortex can be seen end-on in a 71 nm particle at the end of a chain. The positions of the particle's neighbors determine the chirality of the vortex (Fig. 2d), whose core, which is now perpendicular to the chain axis, is only 9±2 nm in diameter. The larger value in Fig. 2a results from dipole-dipole interactions along the chain. These results can be compared with a similar induction map obtained from a chain of $Fe_{10}Ni_{90}$ particles, which is shown in Fig. 2e. The magnetic microstructure in this sample, which has a higher Ni concentration, is closer to that expected for a chain of single-domain spheres. Flux channels, which are 70 nm in diameter, form in this sample only when the particles are above ~100 nm in size.

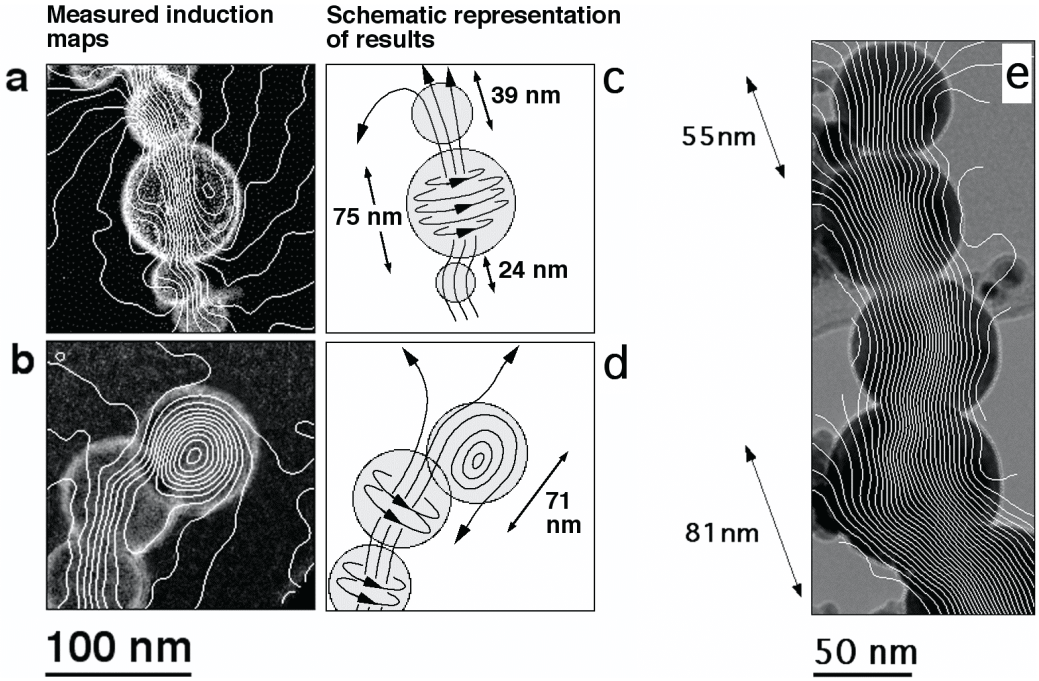

Figure 2 a)-b) Phase contours, which have been overlaid onto O maps, showing the in-plane induction (integrated in the electron beam direction) in chains of $Fe_{55}Ni_{45}$ particles, recorded with the microscope objective lens switched off. The contour spacings are 0.083 and 0.2 radians for a) and b), respectively. The MIP contribution to the phase has been removed from each image. c) and d) show schematic diagrams of the magnetic microstructure in the chains, in which vortices spin around the chain axes. A vortex perpendicular to the chain is also visible in d). e) shows a similar map (spacing 0.125 radians, overlaid onto a bright-field image) from a chain of $Fe_{10}Ni_{90}$ particles.

4. Discussion and Conclusions

The magnetic remanent states shown in Fig. 2 demonstrate the sensitivity of the magnetic microstructure in the FeNi nanoparticle chains to composition, as well as to the sizes and the positions of the particles. Despite the clear trend in the magnetic microstructure with increasing Ni concentration, simple predictions are still complicated by the fact that the critical sizes at which particles cease to be single domain depend not only on their compositions (which affect the exchange length in the alloy) but also on the sizes, compositions and positions of their neighbours. Both high quality magnetic and compositional data and micromagnetic simulations are therefore necessary to understand the magnetic remanent states and reversal mechanisms in such systems fully.

This work was carried out in the framework of the European Research Group "Quantification and measurement in transmission electron microscopy". We thank the Royal Society and Chartered Semiconductor Manufacturing for financial support, and we acknowledge the use of facilities at the Center for High Resolution Electron Microscopy at Arizona State University.

References

[1] P. J. Thomas and P. A. Midgley, Ultramicroscopy **88** (3), 179-186 (2001).
[2] R. E. Dunin-Borkowski and M. R. McCartney, in *Magnetic Nanostructures*, edited by H. S. Nalwa (American Scientific Publishers, 2002), pp. 299-325.
[3] P. Rez, Ultramicroscopy **9** (3), 283-287 (1982).